Nonlinear dynamics of driven superconductors with dissipation

H. P. Ojeda Collado,[1,2] Gonzalo Usaj,[1,2] José Lorenzana,[3] and C. A. Balseiro[1,2]

[1]*Centro Atómico Bariloche and Instituto Balseiro, Comisión Nacional de Energía Atómica (CNEA)–Universidad Nacional de Cuyo (UNCUYO), 8400 Bariloche, Argentina*

[2]*Instituto de Nanociencia y Nanotecnología (INN), Consejo Nacional de Investigaciones Científicas y Técnicas (CONICET)–CNEA, 8400 Bariloche, Argentina*

[3]*ISC-CNR and Department of Physics, Sapienza University of Rome, Piazzale Aldo Moro 2, I-00185, Rome, Italy*

(Received 26 September 2019; revised manuscript received 22 January 2020; accepted 23 January 2020; published 6 February 2020)

In the absence of dissipation a periodically driven BCS superconductor can enter a coherent nonlinear regime of collective Rabi oscillations which last for arbitrary long times [Ojeda Collado *et al.*, Phys. Rev. B **98**, 214519 (2018)]. Here we show that dissipation effects introduce dramatic changes: (i) The collective Rabi mode becomes a transient. (ii) At long times a steady state is reached showing strong nonlinear effects for large enough drive strength. We identify the physical parameters governing the various crossovers and present a detailed computation of time- and angle-resolved photoemission spectroscopy (tr-ARPES) and time-resolved tunneling spectra aiming at detecting the collective Rabi oscillations and the steady-state nonlinearities. We show also that second harmonic generation is allowed for a drive which acts on the BCS coupling constant.

DOI: 10.1103/PhysRevB.101.054502

I. INTRODUCTION

The recent advances in laser technologies have opened new avenues for the study of collective behavior and emergent phenomena in condensed matter [1–9] and ultracold-atom systems [10–15] far from the linear response paradigm. Theoretical examples of these strongly nonlinear phenomena are dynamical phase transitions after a quantum quench [16,17] or under a periodic drive [18].

While these studies are of interest per se, they can also, in principle, shine some light on the nature of the precursor equilibrium phases. In this context, superconducting condensates have drawn increasing attention, both in theoretical and experimental research, as challenging cases for the study of collective out of equilibrium states, especially in the case of superconductors with competing orders [1–9]. Much of the interest in the field was fueled by theoretical studies of quenched systems [16,19,20] and experiments in which the superconductor is excited by a pump pulse without a complete suppression of the superconducting state. In the perturbed system, the superconducting order parameter Δ (Higgs mode) or the charge modes evolve with collective oscillations at frequency 2Δ which are rapidly damped due to dephasing [2,3].

Another interesting way to manipulate a condensate is through periodic drives. In solid-state superconductors, different type of drives have been discussed. Among them are impulsive stimulated Raman scattering (ISRS) [21], phonon assisted modulation of the density of states (DOS driving) as in the case of 2H-$NbSe_2$ [22,23] or of the coupling constant (λ driving) as proposed for FeSe [18], microwave drives and THz drives [24] as already realized in Ref. [4]. Periodic drives can also be implemented in ultracold atoms where there are well known techniques to modify Hamiltonian parameters at will: DOS driving can be achieved modifying the depth of a periodic potential, as it has been done for bosons [10–12]. λ driving can be implemented either by periodically modulating the magnetic field of a Feshbach resonance [13,15] or by radiofrequency dressing with a third state [14].

Previously, we have shown that within a BCS self-consistent dynamics, a periodic excitation at a frequency ω_d in resonance with quasiparticle excitations ($\omega_d > 2\Delta$) can produce collective Rabi oscillations of the quasiparticle population with a frequency proportional to the strength of the drive resulting in a new nonlinear mode of the superconducting order parameter (Rabi-Higgs mode) [18]. This is due to a subset of quasiparticle excitations with energy $E_{\boldsymbol{k}}$ satisfying $\omega_d \approx 2E_{\boldsymbol{k}} = 2\sqrt{\xi_{\boldsymbol{k}}^2 + \Delta^2}$ where $E_{\boldsymbol{k}}$ is the quasiparticle energy and $\xi_{\boldsymbol{k}}$ is the energy of the fermions measured from the chemical potential. A family of quasiparticles approximately satisfying the above condition synchronize among themselves and perform collective oscillations at the Rabi frequency both for λ and DOS driving. Actually, the phenomenon is very general and is expected to occur for any driving that couples with quasiparticles including THz and impulsive stimulated Raman drives (see Appendices A and B of Ref. [18] for an account of various electronic driving mechanisms). Usually the Higgs mode refers to the amplitude mode of the superconducting order parameter which arises because of the broken global U(1) symmetry of the superconducting state [3,4]. Here, Rabi-Higgs refers to a collective mode that corresponds with a modulation of amplitude of the superconducting order parameter (this is why we use the word "Higgs") as a consequence of Rabi oscillations of quasiparticle population in resonance with a periodic drive.

The observation of a Rabi-Higgs mode requires entering into a highly nonlinear regime where damping and

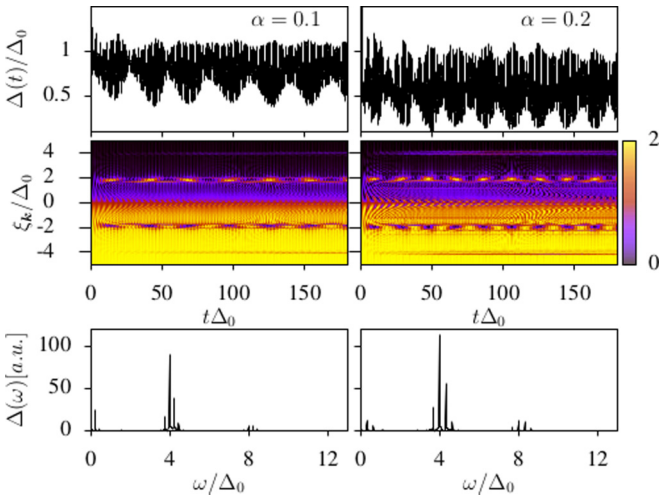

FIG. 1. Superconducting dynamics in the absence of dissipation for $\alpha = 0.1$ (left column) and $\alpha = 0.2$ (right column) and $\omega_d = 4\Delta_0$. From top to bottom we show the superconducting order parameter as a function of time, the time-dependent momentum distribution function $n_k(t)$ and the fast Fourier transform of $\Delta(t)$. We label the states by the normal state quasiparticle energy ξ_k.

decoherence effects can be overcome. One of our goals is to determine under what conditions this regime can be achieved. It is well known from optical Bloch equations for a *single* periodically driven two-level system [25] that a finite energy relaxation time τ leads to a linear response regime for weak excitation amplitudes at long times. The nonlinear regime of Rabi oscillations can be accessed at short times when the Rabi frequency is larger than $1/\tau$. This model has been applied to the case of driven graphene [26] with similar conclusions.

While extrapolation to *many* interacting two-level systems is not granted, in the present work we find that similar regimes do exist in the case of the collective Rabi-Higgs oscillations in BCS superconductors. Therefore, their observation requires long relaxation times and/or strong drives (which result in Rabi-Higgs frequency $\Omega_R > 1/\tau$).

How long can τ be in superconductors? It is known that quasiparticle relaxation times can be extremely long under favorable conditions. A simple estimate can be obtained through the Dynes parameter [27] in tunneling experiments which, as explicitly shown in Ref. [28], is directly related to the damping of quasiparticles by the bath ultimately limiting the coherent dynamics. In aluminium samples, an inverse Dynes parameter $1/\gamma \equiv \tau \sim 10^6/\Delta \sim \mu$s has been measured [29] which suggests that there is a large time window for coherent dynamics. Indeed, we found that for a moderate drive strength the Rabi period $\tau_R \equiv 2\pi/\Omega_R$ is in the scale of tenths or hundreds of $1/\Delta \ll \tau$ (see Fig. 1). On the other hand, the above estimate for τ is probably too optimistic as the same out-of-equilibrium quasiparticles will open new relaxation channels [30] and hence the whole out-of-equilibrium many-body problem should be considered in a self-consistent manner.

Here we take a simple approach for the interplay of coherent nonlinear phenomena and damping by considering a driven superconductor in the presence of a bath providing energy relaxation. We make the simplest possible assumption for the bath leaving a microscopic many-body description for future work. Thus we treat the coupling with the bath as a phenomenological parameter and present the spectral signatures of the Rabi-Higgs modes varying the coupling and other experimental parameters. Differently from previous works, and as a first step towards a full many-body treatment, the dissipative dynamics is treated in a self-consistent way using the method introduced in Ref. [28]. Both tr-ARPES and tunneling are analyzed in detail. Signature of the Rabi-Higgs oscillations are accessible in both experiments at short times. At long times a steady state is achieved with interesting nonlinear phenomena also amenable to experimental investigation as second-harmonic generation and population imbalance saturation.

II. THE TIME-DEPENDENT BCS MODEL WITH DISSIPATION

In the absence of dissipation, λ drive and DOS drive produce qualitatively similar results [18]. As we expect the same to be true in the presence of dissipation, we restrict hereon to study λ driving.

In addition, in the dissipationless case, even for weak drives and for $\omega_d > 2\Delta$ the Rabi-Higgs mode appears with frequency Ω_R proportional to the intensity of the drive. Apparently the Rabi-Higgs mode violates any linear response prescription. Indeed, as mentioned in the introduction, without dissipation the system becomes inherently nonlinear at long times no matter how weak the perturbation is. In analogy with two-level systems we expect that dissipation effects redress this anomalous behavior. This would imply that the order of limits is important. Taking first the Rabi frequency (proportional to the drive intensity) $\Omega_R \to 0$ and then energy relaxation times $\tau \to \infty$ a linear response regime should be well defined. Inverting the order of limits it should not. The numerical results below are consistent with this theoretical expectation.

A. Model and formalism

We consider a single-band s-wave superconductor described by the Hamiltonian,

$$H_{\rm BCS} = \sum_{\boldsymbol{k},\sigma} \xi_{\boldsymbol{k}} c^\dagger_{\boldsymbol{k}\sigma} c_{\boldsymbol{k}\sigma} - \lambda(t) \sum_{\boldsymbol{k},\boldsymbol{k}'} c^\dagger_{\boldsymbol{k}\uparrow} c^\dagger_{-\boldsymbol{k}\downarrow} c_{-\boldsymbol{k}'\downarrow} c_{\boldsymbol{k}'\uparrow} \quad (1)$$

where $c_{\boldsymbol{k}\sigma}$ ($c^\dagger_{\boldsymbol{k}\sigma}$) destroys (creates) an electron with momentum $\boldsymbol{k}$, energy $\varepsilon_{\boldsymbol{k}}$, and spin σ. Here $\xi_{\boldsymbol{k}} = \varepsilon_{\boldsymbol{k}} - \mu$ measures the energy from the Fermi level μ and the pairing interaction $\lambda(t)$ is parameterized as

$$\lambda(t) = \lambda_0[1 + \Theta(t)\alpha \sin(\omega_d t)], \quad (2)$$

where $\Theta(t)$ is the Heaviside step function. In most of our calculations we take the parameter $\alpha \in [0, 0.2]$ that corresponds to a modulation of up to 20% of the equilibrium pairing interaction λ_0, to keep it within the range of experimental accessibility in condensed matter systems assuming a phonon-assisted λ-driving mechanism [18,31]. In the thermodynamic limit, the Hamiltonian (1) is equivalent to the mean-field

Hamiltonian,

$$H_{\rm MF} = \sum_{\boldsymbol{k}} \psi^{\dagger}_{\boldsymbol{k}} \boldsymbol{H}_{\boldsymbol{k}}(t) \psi_{\boldsymbol{k}}, \tag{3}$$

written in the Nambu spinor basis $\psi_{\boldsymbol{k}} = (c_{\boldsymbol{k}\uparrow}, c^{\dagger}_{-\boldsymbol{k}\downarrow})^{\rm T}$, where

$$\boldsymbol{H}_{\boldsymbol{k}}(t) = \begin{pmatrix} \xi_{\boldsymbol{k}} & -\Delta(t) \\ -\Delta(t)^* & -\xi_{\boldsymbol{k}} \end{pmatrix}, \tag{4}$$

and the instantaneous superconducting order parameter is given by

$$\Delta(t) = \lambda(t) \sum_{\boldsymbol{k}} \langle c^{\dagger}_{\boldsymbol{k}\uparrow}(t) c^{\dagger}_{-\boldsymbol{k}\downarrow}(t) \rangle. \tag{5}$$

Here $\langle \ldots \rangle$ denotes the expectation value on the initial state. Notice that the expectation value on the right hand side of Eq. (5) is in the Heisenberg picture so the full many-body time evolution is taken into account by the unitary evolution of the operators. Despite the simplicity of the drive Eq. (2), we will see that $\Delta(t)$ can develop quite complex phenomena with different frequencies entering into play in a self-consistent manner.

In order to consider dissipation we couple the superconductor to a reservoir. For simplicity we will take the bath to be at zero temperature, which means that if the superconductor is out of equilibrium at some time and it is allowed to evolve in the absence of the drive, it will eventually relax to the ground state with the bath absorbing all the excess energy. The method to treat the bath was explained in detail in Ref. [28]. Here we summarize the main results.

To describe the reservoir effect, the self-consistent solution of the gap equation is written in terms of the Keldysh two-time contour Green's functions. In the Nambu spinor basis, the retarded and lesser Green functions are 2×2 matrices with matrix elements given by

$$\begin{aligned} \boldsymbol{G}^{R}_{\boldsymbol{k}}(t,t')_{\alpha\beta} &= -i\Theta(t-t')\langle \{\psi_{\boldsymbol{k}\alpha}(t), \psi^{\dagger}_{\boldsymbol{k}\beta}(t')\}\rangle, \\ \boldsymbol{G}^{<}_{\boldsymbol{k}}(t,t')_{\alpha\beta} &= i\langle \psi^{\dagger}_{\boldsymbol{k}\alpha}(t')\psi_{\boldsymbol{k}\beta}(t)\rangle, \end{aligned} \tag{6}$$

respectively, here $\{,\}$ denotes the anticommutator. Thus, the superconducting gap equation [Eq. (5)] can be written as

$$\Delta(t) = -i\lambda(t) \sum_{\boldsymbol{k}} \boldsymbol{G}^{<}_{\boldsymbol{k}}(t,t)_{12}. \tag{7}$$

When considering the coupling to a reservoir, the lesser Green function satisfies the Keldysh equation in time domain [28,32–34]

$$\boldsymbol{G}^{<}_{\boldsymbol{k}}(t,t') = \int dt_1 \int dt_2\, \boldsymbol{G}^{R}_{\boldsymbol{k}}(t,t_1)\boldsymbol{\Sigma}^{<}_{\boldsymbol{k}}(t_1,t_2)\boldsymbol{G}^{R}_{\boldsymbol{k}}(t',t_2)^{\dagger} \tag{8}$$

where the dissipation effects are taken into account via the lesser self-energy $\boldsymbol{\Sigma}^{<}_{\boldsymbol{k}}(t_1,t_2)$ and the retarded Green function which is solution of the corresponding Dyson equation with a retarded self-energy $\boldsymbol{\Sigma}^{R}_{\boldsymbol{k}}(t_1,t_2)$.

Following Refs. [34,35] we consider a mechanism for dissipation that couples each pair of states $\boldsymbol{k}\uparrow, -\boldsymbol{k}\downarrow$ with a reservoir described by a time-independent one body Hamiltonian $H_b = \sum_{\ell,\sigma} E_\ell d^{\dagger}_{\ell\sigma} d_{\ell\sigma}$ where $d^{\dagger}_{\ell\sigma}$ creates an electron in a single particle bath state with energy E_ℓ. In the limit of a wide-band reservoir with identical coupling $V_{k\ell} = V_\ell$ for each $\boldsymbol{k}$ all details of the bath band structure disappear and its effects can be described by a single frequency independent parameter γ describing the effects of inelastic scattering, producing a level broadening $\sim\gamma$ and a finite lifetime $\tau = 1/\gamma$. The generalization to the case of a $\boldsymbol{k}$-dependent lifetime $\gamma_{\boldsymbol{k}}$ is straightforward and undemanding, however taking a constant γ is good approximation as all the physical process take place in a narrow energy window around the Fermi energy.

In this formulation, the retarded and lesser self-energy become momentum independent and diagonal in Nambu space, i.e., $\boldsymbol{\Sigma}^{R}_{\boldsymbol{k}} \equiv \mathbf{I}\Sigma^{R}$ and $\boldsymbol{\Sigma}^{<}_{\boldsymbol{k}} \equiv \mathbf{I}\Sigma^{<}$ with

$$\begin{aligned} \Sigma^{R}(t_1,t_2) &= -i\gamma\delta(t_1-t_2)/2, \\ \Sigma^{<}(t_1,t_2) &= i\gamma \int \frac{d\omega}{2\pi} f(\omega) e^{-i\omega(t_1-t_2)}. \end{aligned} \tag{9}$$

Here $f(\omega)$ is the Fermi function evaluated at the bath temperature. Consequently, the Dyson equation for the retarded Green function can be easily integrated, being given by $\boldsymbol{G}^{R}_{\boldsymbol{k}}(t,t') = \boldsymbol{G}^{R(0)}_{\boldsymbol{k}}(t,t')e^{-\gamma(t-t')/2}$ where $\boldsymbol{G}^{R(0)}_{\boldsymbol{k}}(t,t')$ is the retarded Green function in the absence of dissipation. The latter can be computed by solving the following differential equations (in matrix notation in the Nambu spinor basis and setting $\hbar = 1$),

$$\begin{aligned} \boldsymbol{G}^{R(0)}_{\boldsymbol{k}}(t,t) &= -i\boldsymbol{I}, \\ i\partial_t \boldsymbol{G}^{R(0)}_{\boldsymbol{k}}(t,t') &= \boldsymbol{H}_{\boldsymbol{k}}(t)\boldsymbol{G}^{R(0)}_{\boldsymbol{k}}(t,t'), \quad t > t', \\ i\partial_{t'} \boldsymbol{G}^{R(0)}_{\boldsymbol{k}}(t,t') &= -\boldsymbol{G}^{R(0)}_{\boldsymbol{k}}(t,t')\boldsymbol{H}_{\boldsymbol{k}}(t'), \quad t > t'. \end{aligned} \tag{10}$$

Replacing Eq. (9) into Eq. (8) and assuming a reservoir at zero temperature we obtain

$$\begin{aligned} \boldsymbol{G}^{<}_{\boldsymbol{k}}(t,t') = -\frac{\gamma}{2\pi} \int_{-\infty}^{t} dt_1 \int_{-\infty}^{t'} dt_2 \boldsymbol{G}^{R(0)}_{\boldsymbol{k}}(t,t_1)\boldsymbol{G}^{R(0)}_{\boldsymbol{k}}(t',t_2)^{\dagger} \\ \times \frac{e^{-\gamma(t-t_1+t'-t_2)/2}}{t_1 - t_2 + i0^+}. \end{aligned} \tag{11}$$

Hence, the time dependence of the order parameter [Eq. (7)] can be obtained after computing the lesser Green function [Eq. (11)] for $t' = t$. This equal-time lesser Green function $\boldsymbol{G}^{<}_{\boldsymbol{k}}(t,t) \equiv \boldsymbol{G}^{<}_{\boldsymbol{k}}(t)$ satisfies the equation of motion

$$\partial_t \boldsymbol{G}^{<}_{\boldsymbol{k}}(t) = -\gamma \boldsymbol{G}^{<}_{\boldsymbol{k}}(t) + \boldsymbol{\mathcal{I}}_{\boldsymbol{k}}(t) - i[\boldsymbol{H}_{\boldsymbol{k}}(t), \boldsymbol{G}^{<}_{\boldsymbol{k}}(t)], \tag{12}$$

where

$$\boldsymbol{\mathcal{I}}_{\boldsymbol{k}}(t) = \frac{i\gamma}{2\pi} \int_{-\infty}^{t} dt' \left(\frac{\boldsymbol{G}^{R(0)}_{\boldsymbol{k}}(t,t')}{t-t'-i0^+} + \frac{\boldsymbol{G}^{R(0)}_{\boldsymbol{k}}(t,t')^{\dagger}}{t-t'+i0^+} \right) e^{-\frac{\gamma(t-t')}{2}}. \tag{13}$$

The initial condition for the differential Eq. (12) is given by the equilibrium value of the lesser Green function

$$\boldsymbol{G}^{<}_{\boldsymbol{k}}(0) = \frac{i}{2}\boldsymbol{I} - \frac{i}{\pi E_{\boldsymbol{k}}} \arctan\left(\frac{2E_{\boldsymbol{k}}}{\gamma}\right) \begin{pmatrix} \xi_{\boldsymbol{k}} & -\Delta_0 \\ -\Delta_0 & -\xi_{\boldsymbol{k}} \end{pmatrix}, \tag{14}$$

where $E_{\boldsymbol{k}} = \sqrt{\xi^2_{\boldsymbol{k}} + \Delta^2_0}$, which is time independent and easily obtained after replacing the equilibrium retarded Green function in Eq. (11) (see Ref. [28]). As a consequence, in the presence of dissipation, the equilibrium order parameter Δ_0 is

defined, via Eq. (7), by the gap equation

$$1 = \frac{1}{\pi}\sum_{k}\frac{\lambda_0}{E_k}\arctan\left(\frac{2E_k}{\gamma}\right). \tag{15}$$

In the $\gamma \to 0$ limit Eq. (15) becomes the standard BCS gap equation. In the presence of inelastic scattering ($\gamma \neq 0$) the superconducting order parameter is reduced. As already mentioned, another important result is that at equilibrium the present formalism presents a rigorous justification for the Dynes formula for the density of states [28]. As will be shown explicitly below, this provides a simple way to estimate the γ parameter close to equilibrium directly from tunneling experiments [27,29].

B. Rabi-Higgs modes in the superconducting response and dissipation effects

We now present the numerical solution of our model for λ driving. For concreteness we shall show simulations for $\omega_d = 4\Delta_0$ but qualitative similar behavior is obtained for not too large frequencies above the gap ($\omega_d > 2\Delta_0$).

At $t \leqslant 0$ the system is in equilibrium and the order parameter Δ_0 is given by Eq. (15). At $t > 0$ the drive switches on according to Eq. (2) and we compute the equal-time lesser Green function via Eqs. (12)–(14) in order to self-consistently determine the superconducting order parameter evolution through Eq. (7).

1. Nonlinear effects in the undamped dynamics

Here we briefly present the superconducting response in the absence of dissipation aiming at: (a) showing that the formulation in terms of the Keldysh Green functions reproduces the known results [18] obtained with the simpler Anderson's pseudospins description, (b) discussing the occurrence of an anomalous second harmonic generation, and (c) presenting results to compare with those in which the reservoir effects play a role.

In the absence of dissipation the calculation is made by considering the evolution of the equal-time lesser Green function dictated only by the commutator with the Hamiltonian [Eq. (12) without the two first terms in the r.h.s.]. The dynamics of $\Delta(t)$ and the expectation value of the momentum distribution function,

$$n_{\boldsymbol{k}}(t) = \sum_{\sigma}\langle c^{\dagger}_{\boldsymbol{k}\sigma}(t)c_{\boldsymbol{k}\sigma}(t)\rangle = 1 - i[\boldsymbol{G}^{<}_{\boldsymbol{k}}(t)_{11} - \boldsymbol{G}^{<}_{\boldsymbol{k}}(t)_{22}] \tag{16}$$

are shown in Fig. 1 for two different values of the perturbation amplitude α. It is apparent from the figure that the order parameter oscillates with two fundamental frequencies and, after a short transient, averages to a smaller value with respect to equilibrium. The drive frequency corresponds to a fast oscillation that cannot be resolved on the scale of the figure and leads to the filled black regions of the gap dynamic. In addition, the amplitude of the gap shows the Rabi-Higgs oscillations with a frequency that increases approximately linearly with increasing α. Indeed,

$$\frac{\Omega_R}{\Delta_0} \approx A(\omega_d/\Delta_0)\alpha \tag{17}$$

with

$$A(\omega_d/\Delta_0) = \frac{\sqrt{1-\left(\frac{2\Delta_0}{\omega_d}\right)^2}}{1 - 2\lambda_0\chi^0_{\Delta,\Delta}(\omega_d)} \tag{18}$$

where $\chi^0_{\Delta,\Delta}(\omega_d)$ is a bare susceptibility that takes into account how the system respond to a periodic time-dependent stimuli of frequency ω_d (see Ref. [18] for an analytic approximation for this susceptibility using linear response).

The Rabi-Higgs mode is associated with a periodic inversion of the population of the quasiparticles in resonance with the drive. For $\omega_d = 4\Delta_0$, this is visible in the momentum distribution function $n_{\boldsymbol{k}}(t)$ as a narrow time dependent structure at quasiparticle energy $\xi_{\boldsymbol{k}} \approx \pm 2\Delta_0$ (Fig. 1, middle panel) with a frequency that matches the Rabi-Higgs period of $\Delta(t)$. Notice that the inversion of colors along the anomaly represent a cyclic inversion of population of the resonant quasiparticles. Such a time-dependent anomaly represents a clear hallmark of the Rabi-Higgs mode and opens the possibility to detect it through spectroscopies as we shall demonstrate in the next section.

Another nonlinear effect is the generation of a second harmonic and its associated Rabi-Higgs mode. In the case of an electromagnetic drive, second harmonic generation is not allowed [36]. This follows from the general fact that the current response to the vector potential A is $J \sim \rho_s(A)A$ where $\rho_s(A)$ is the superfluid stiffness. In the absence of a steady state current, the free energy and $\rho_s(A)$ are even in A, so the lowest nonlinear contribution to J is order A^3, i.e., third harmonic generation [36]. In contrast, such symmetry does not exist in our case since for $\lambda > 0$, terms odd in $\delta\lambda$ are allowed in the free energy and second harmonic generation is possible. Indeed, as can be seen in the bottom panel of Fig. 1 the superconducting response not only contains the driving frequency $\omega_d = 4\Delta_0$ but also $2\omega_d = 8\Delta_0$. This can also be seen in the middle panel of Fig. 1, where a less intense Rabi-Higgs mode is developed, associated with the second harmonic response, i.e., quasiparticles with $\xi_{\boldsymbol{k}} \approx \pm 4\Delta_0$ show a narrow time dependent anomaly in the population but with a much smaller Rabi frequency.

2. Dissipative dynamics

We now present one of the central results of this contribution: the effect of dissipation on the Rabi-Higgs mode and in general on the charge dynamics. As mentioned in the introduction, we know from Bloch equations for a single two-level system that the Rabi oscillation becomes a transient effect in the presence of dissipation. The driven superconducting response [$\Delta(t)$] in the presence of a bath is shown in Fig. 2 for different values of the bath parameter γ and the perturbation amplitude α. We see that also the collective Rabi oscillations of many interacting and synchronized two-level systems become a transient effect in the presence of dissipation. Indeed, for sufficiently long times a steady state is achieved where only the drive frequency is present.

As γ is increased (from top to bottom in Fig. 2) the system reaches a steady state more rapidly with a vanishing of Rabi-Higgs oscillations. By increasing α, for a fixed value of γ, Ω_R increases [cf. Eq. (17)] and several Rabi-Higgs

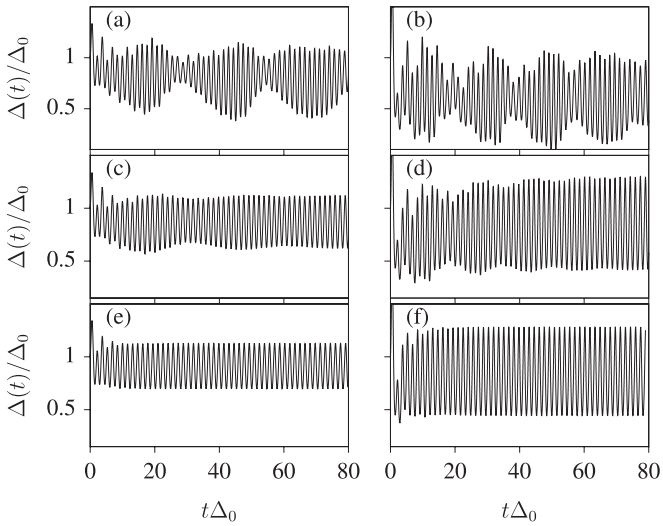

FIG. 2. Time dependence of the superconducting order parameter in the presence of dissipation for $\alpha = 0.1$ (left column) and $\alpha = 0.2$ (right column). From top to bottom we use $\gamma = 0$ (without dissipation effects), $\gamma = 0.05\Delta_0$ and $\gamma = 0.2\Delta_0$, respectively.

oscillations are visible before they disappear as a consequence of relaxation [see, for example, Figs. 2(c) and 2(d)]. Thus, in order to detect the Rabi-Higgs modes experimentally it is necessary to ensure that $\Omega_R \gtrsim \gamma$. In fact, for the γ values used here, the slower Rabi-Higgs mode, associated with the second harmonic generation (Sec. II B 1), is not visible.

Conversely, for small α and strong dissipation it is possible to get $\Omega_R \lesssim \gamma$ and only oscillations in synchrony with the drive are visible as expected from linear response theory (bottom panels of Fig. 2 and Fig. 3). In this regime, the amplitude of the oscillation in the order parameter increases linearly with α as shown in Fig. 3. However, it is important to note that by increasing α, and after a very fast transient, the superconducting gap decreases in average which constitutes the first steady-state nonlinear effect arising in the dynamics.

As a conclusion, in the presence of dissipation, we can distinguish two different main regimes: For $\Omega_R \lesssim \gamma$ there are no Rabi oscillations and linear response theory can be applied even at short times. For $\Omega_R \gtrsim \gamma$ Rabi-Higgs oscillations can be observed as a transient phenomena. In both cases, a steady-state nonlinear regime appears at large fields

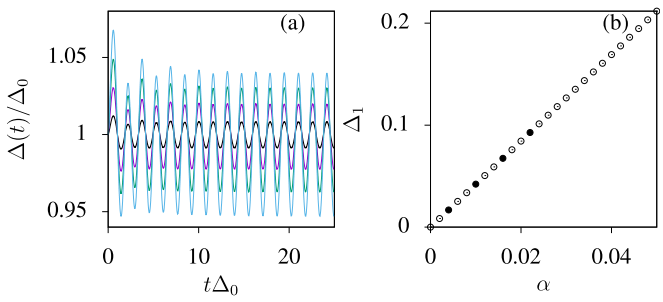

FIG. 3. (a) Time dependence of the order parameter for $\gamma = 0.2\Delta_0$ and $\alpha = 0.004, 0.01, 0.016, 0.022$. (b) Amplitude of the oscillation in the order parameter Δ_1 as a function of the strength of the drive α. The filled points correspond with the curves of panel (a).

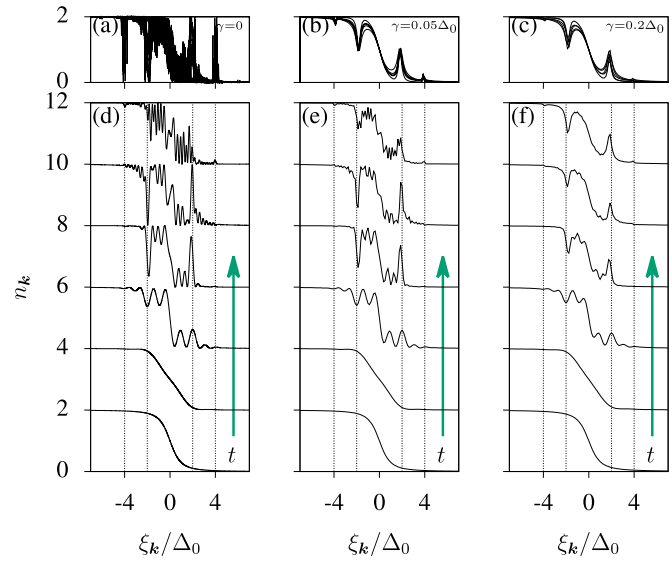

FIG. 4. n_k distribution as a function of time for $\alpha = 0.2$ and $\gamma = 0$ (left column), $\gamma = 0.05\Delta_0$ (middle column), and $\gamma = 0.2\Delta_0$ (right column). In panels (d)–(f), the time increases from bottom to top as follows $t = 0$ (equilibrium), $t = 0.1\tau_R$, $t = 0.25\tau_R$, $t = 0.5\tau_R$, $t = 0.75\tau_R$, and $t = \tau_R$ (Rabi-Higgs period $\tau_R\Delta_0 = 15$). For clarity, the zero of each curve was displaced vertically by 2 units. The oscillating n_k distributions in the steady state are shown in panels (a)–(c) at different times within a drive period. Notice that for $\gamma = 0$ the steady-state shows Rabi oscillations. In panel (a) the curves are shown when population inversion is maximum.

which is also interesting. Below we will explore both; the transient nonlinear regime for $2\pi/\Omega_R < t_M < 1/\gamma$, with t_M the measurement time, and the steady-state nonlinear regime for large drive amplitude and $t_M > 1/\gamma$.

We start discussing in more detail the transient nonlinear regime, in particular the possibility of detection of the Rabi-Higgs mode in experiments. Previously, we have demonstrated that the Rabi-Higgs mode is associated with oscillations in the occupation values n_k (see Fig. 1). These charge fluctuations provide an efficient manner to detect the existence of this nonlinear mode with standard experimental techniques as we shall show in the next section.

Since for the simple electronic structure we are taking, n_k depends on $\boldsymbol{k}$ only through its distance from the Fermi surface (ξ_k) it is useful to introduce the distribution function $n(\xi_k) \equiv n_k$. When convenient, in the following we will drop the momentum dependence and refer to $n(\xi)$ loosely as the "momentum distribution function" keeping in mind the above equivalence.

In Fig. 4 we show the time-dependent n_k distribution taking into account dissipative effects (middle and right column) in comparison with the dissipationless counterpart (left column) at different times within the first Rabi cycle [panels (d)–(f)] and in the steady state [panels (a)–(c)]. We have used the same γ and α parameters as in the right column of Fig. 2.

For $\gamma = 0$ the Rabi oscillations can be observed as oscillations in the occupation value n_k for $\xi_k \approx \pm 2\Delta_0$, which we will refer to as $n(\pm\xi_R)$. Small peaks also appear for $\xi_k \approx \pm 4\Delta_0$, corresponding to the second-harmonic slower Rabi-Higgs mode that starts to develop in the temporal window

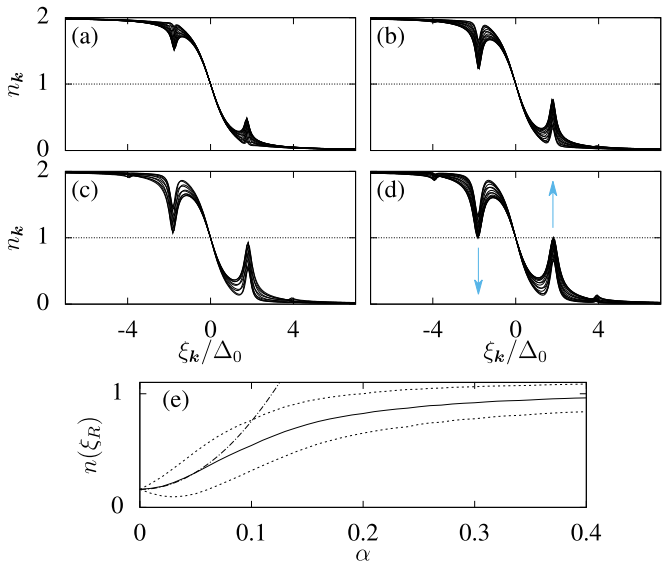

FIG. 5. Steady-state n_k distributions for $\gamma = 0.2\Delta_0$ and $\alpha = 0.05$ (a), $\alpha = 0.1$ (b), $\alpha = 0.15$ (c), and $\alpha = 0.2$ (d). In panel (e) the dashed and solid lines represent the (minimum, maximum) and average value of $n(\xi_R)$, respectively, as a function of α. Notice that $n(\xi_R)$ is nonzero even for $\alpha = 0$ as an excess of occupation is inherent to the BCS ground state. The dot-dashed line is a quadratic fitting for the average of excited population for small α values. The population inversion starts when $n(\xi_R)$ exceeds the horizontal line $n_k = 1$ which is represented with arrows in the panel (d). As a consequence of the presence of dissipation, in the steady state regime this does not occur not matter how strong the perturbation is.

used in Fig. 4(d). At long times, the two Rabi-Higgs modes can be seen as is shown in Fig. 4(a).

In the presence of weak dissipation ($\gamma = 0.05\Delta_0$), the transient dynamic only shows oscillations of $n(\pm\xi_R)$, corresponding to the fastest Rabi-Higgs mode. Finally, for strong dissipation ($\gamma = 0.2\Delta_0$), a full Rabi cycle cannot be completed since the relaxation takes place in a very short time. As a consequence $n(\xi_R)$ [$n(-\xi_R)$] increases (decreases) during a short period of time and rapidly saturates without exhibiting Rabi oscillations.

The n_k distribution in the steady state in the presence of dissipation are shown in Figs. 4(b) and 4(c) for different times within a period of the drive. In this case, n_k shows a peak at $\xi_k \approx \pm 2\Delta_0$ such that $n(\pm\xi_R) \approx 1$ all the time. Taking into account spin this corresponds to half-filled single particle states. Below we will show that the present value of $\alpha = 0.2$ is large enough to be in the steady-state nonlinear regime. Thus, ultimately the fate of the superconducting dynamics is a gap oscillation with the drive frequency [see Figs. 2(e) and 2(f)] and a quasi-stationary population unbalance at the quasiparticle energy ξ_R.

Now we focus on the steady-state regime after the transient to identify the crossover between linear and nonlinear regime. We have extracted the n_k distribution at long times for several values of α with $\gamma = 0.2\Delta_0$. The population unbalance changes considerably as a function of the amplitude of the perturbation as can be appreciated in Fig. 5. This phenomenon is well known in nonlinear quantum optics. There, one usually considers a two-level system in the presence of a driving force and damping effects via a phenomenological parameter in the Bloch equation of motion. For a drive frequency in resonance with the two level system, the excited population in the steady state increases with the amplitude of the perturbation and in the limit of large intensity, the largest possible excited population is equal to the ground state population [25] (on passing we notice that other outcomes are possible relaxing the wide-band bath condition [37]).

As already mentioned, the present context is quite different from quantum optics because the phenomenon does not correspond to a single two-level system but a collection of two-level systems interacting through the self-consistency that determines the superconducting order parameter. Despite that, we find that in the limit of large α [Fig. 5(e)] the steady state population saturates at the half-filled value (counting spin) $n(\xi_R) \approx 1$. In other words, as for a single two-level system, there is never a steady state with population inversion [e.g., a sign change of $n(\xi_R) - n(-\xi_R)$] no matter how large α is.

The above results show that nonlinearities are controlled in a similar manner as for single two-level systems. Assuming this analogy, the linear response regime is characterized by off-diagonal elements of the density matrix linear in α and diagonal elements quadratic in α (as dictated by symmetry). Indeed, one sees that for small α values the average population imbalance [full line in Fig. 5(e)] is quadratic in α. Around $\alpha \sim 0.1$ this regime breaks down and the system crosses over to the nonlinear steady-state regime. Thus the steady-state linear regime requires $\alpha \ll 1$ or equivalently $\Omega_R \ll \Delta_0$ [cf. Eq. (17)].

III. THEORETICAL MODELING OF TR-ARPES AND TUNNELING EXPERIMENTS: SPECTRAL FINGERPRINTS OF RABI-HIGGS MODE

Our main aim in this section is to identify some spectral fingerprints giving experimental access to the interesting nonlinear regimes we have identified in the previous sections in the presence of dissipation, the transient nonlinear regime (Rabi-Higgs mode), and the steady-state nonlinear regime. Clearly, an emergent technique to detect transient phenomena is tr-ARPES and so we discuss such a case first. Yet, in addition, we shall demonstrate that also time resolved tunneling experiments could be useful to detect the nonlinear mode discussed above. In all the calculations discussed below, we obtain the spectral signals in terms of the lesser Green function Eq. (11) as a function of α and γ.

A. tr-ARPES

In our setting the λ driving is turned on at time $t = 0$ and the photoemission process is induced by a wave packet of photons centered at time t_0 and with central energy $\hbar\omega_q$ larger than the work function of the solid W. For simplicity we use a Gaussian shape for this probe pulse, $s(t) = \exp(-(t - t_0)^2/2\sigma^2)/(\sigma\sqrt{2\pi})$ with standard deviation σ.

In a tr-ARPES experiment the momentum of the outgoing electrons $\boldsymbol{k}_e$ is measured. Energy conservation determines the excitation energy left in the system after the photoemission process, $\hbar\omega = \hbar\omega_q - (\hbar k_e)^2/(2m_e) - W$ and momentum

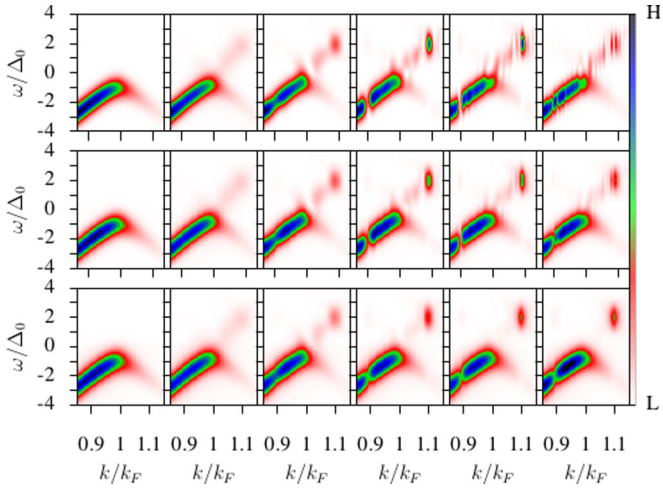

FIG. 6. tr-ARPES intensity for $\alpha = 0.2$ at several photoemission times inside the first period τ_R of Rabi-Higgs mode, from left to right, $t_0 = 0$ (equilibrium), $t_0 = 0.1\tau_R$, $t_0 = 0.25\tau_R$, $t_0 = 0.5\tau_R$, $t_0 = 0.75\tau_R$, and $t_0 = \tau_R$. From top to bottom we show results for $\gamma = 0$ (without dissipation), $\gamma = 0.05\Delta_0$, and $\gamma = 0.2\Delta_0$ as in Fig. 2.

conservation yields information on the momentum of the excitations $\boldsymbol{k}$. The momentum resolved photocurrent in the detector at time t is due to all electrons photoemitted before such time and is determined by [38]

$$I_{\boldsymbol{k}}(\omega, t) = \mathrm{Im}\int_{-\infty}^{t} dt_1 \int_{-\infty}^{t} dt_2 s(t_1)s(t_2)e^{i\omega(t_1-t_2)}\boldsymbol{G}^{<}_{\boldsymbol{k}}(t_1, t_2)_{11}. \tag{19}$$

In order to probe the Rabi-Higgs modes in real time in the following we use different probe times t_0 and take the integration limit from a lower cutoff time $t_l = t_0 - 5\sigma$ to $t = t_0 + 5\sigma$. Figure 6 shows the tr-ARPES intensity with and without dissipation for different t_0 during the first period τ_R associated with the Rabi-Higgs mode. For simplicity, we consider a parabolic band for electrons $\xi_{\boldsymbol{k}} \propto (k^2 - k_F^2)$ and use a probe pulse with a standard deviation $\sigma = 0.1\tau_R$. From the photoemission signal at equilibrium (left column in Fig. 6) there is an almost imperceptible broadening of the spectral line as γ is increased, which leads to a decrease of superconducting order parameter according to Eq. (15).

The presence of Rabi-Higgs oscillations are clearly visible in the top and middle panels of Fig. 6 via a spectral weight around $\omega = \pm 2\Delta_0$ that increases (decreases) above (below) the Fermi energy in the first half period and has the opposite behavior in the second half period of the Rabi-Higgs mode. One can visualize the process as an excitation of quasiparticles from the lower quasiparticle branch to the higher quasiparticle branch in the first half cycle followed by a deexcitation in the second half cycle or equivalently as a stimulated absorption phase followed by a stimulated emission phase. If γ is large enough, Rabi oscillations are not visible and only the spectral weight corresponding with the steady state is observed after a fast transient (bottom panel of Fig. 6).

Clearly the above dynamics is the photoemission image of the momentum distribution function imbalance discussed above. Indeed, integrating in frequency

$$\int_{-\infty}^{\infty} \frac{d\omega}{2\pi} I_{\boldsymbol{k}}(\omega, t) = \mathrm{Im}\int_{-\infty}^{t} dt' s(t')^2 \boldsymbol{G}^{<}_{\boldsymbol{k}}(t', t')_{11}$$
$$= \frac{1}{2}\int_{-\infty}^{t} dt' s(t')^2 n_{\boldsymbol{k}}(t') \tag{20}$$

which is clearly a moving average of $n_{\boldsymbol{k}}(t)$. For example, in the large γ case the unbalance over time in the tr-ARPES intensity for $\omega = \pm 2\Delta_0$ matches the $n_{\boldsymbol{k}}$ distribution in the steady state shown in Fig. 5(d). It is interesting that in photoemission spectral weight is transferred from small momentum to large momentum which is clearly associated with the rearrangement of the momentum distribution function. Such rearrangement of the spectral weight is a hallmark of the effects discussed and establishes tr-ARPES experiments as a tool to investigate steady-state nonlinearities, like population imbalance, and transient nonlinearities like the Rabi-Higgs mode, in driven superconductors.

Floquet analysis of the steady state regime

As already mentioned for $t \gtrsim \tau = 1/\gamma$ one reaches a steady state and the superconducting gap oscillates only with the drive frequency. Therefore the mean-field Hamiltonian Eq. (3) is time periodic at long times and we can use Floquet theorem to analyze the spectrum. This theorem guarantees the existence of a set of solutions of the time-dependent Schrodinger equation of the form

$$|\psi_\nu(t)\rangle = \exp(-i\varepsilon_\nu t/\hbar)|\phi_\nu(t)\rangle \tag{21}$$

where $|\phi_\nu(t)\rangle$ has the same periodicity of the Hamiltonian Eq. (4) [39,40]. The Floquet states $|\phi_\nu(t)\rangle$ are the solutions of

$$\mathcal{H}_F|\phi_\nu(t)\rangle = \varepsilon_\nu|\phi_\nu(t)\rangle \tag{22}$$

where $\mathcal{H}_F = H_{\mathrm{MF}} - i\hbar\partial/\partial t$ is the Floquet Hamiltonian and ε_ν is the quasienergy [41,42]. In the Floquet basis this Hamiltonian becomes a time-independent infinite matrix operator. Since we are interested in the low quasienergy spectra we restrict the Floquet Hamiltonian to a large enough but finite subspace containing many multiphoton processes (finite number of replicas) [41,42].

For $\gamma = 0.2\Delta_0$ and $\alpha = 0.2$ the steady-state condition is reached already for $t \sim 0.75\tau_R = 11.25/\Delta_0$. The quasienergy spectrum in the long time limit is well described by $\Delta(t) = \bar{\Delta} + \Delta_1 \cos(\omega_d t)$ with $\bar{\Delta} = 0.86\Delta_0$ and $\Delta_1 = 0.42\Delta_0$ [cf. Fig. 2(f)].

In the upper panels of Fig. 7 we compare the tr-ARPES with the Floquet spectrum in the steady state. To analyze the details, in the right panels we sacrifice temporal resolution to gain energy resolution by using a wider probe pulse. We see that the tr-ARPES signal nicely matches the Floquet spectrum, depicted by the dashed line. Thus the tr-ARPES signal essentially probes the occupied parts of the Floquet band structure.

Surprisingly, also in the transient dynamics the tr-ARPES intensity fits very well with a Floquet spectrum that is obtained from an effective $\Delta(t)$ with a monochromatic dependence (see lower panel of Fig. 7), even thought in this regime

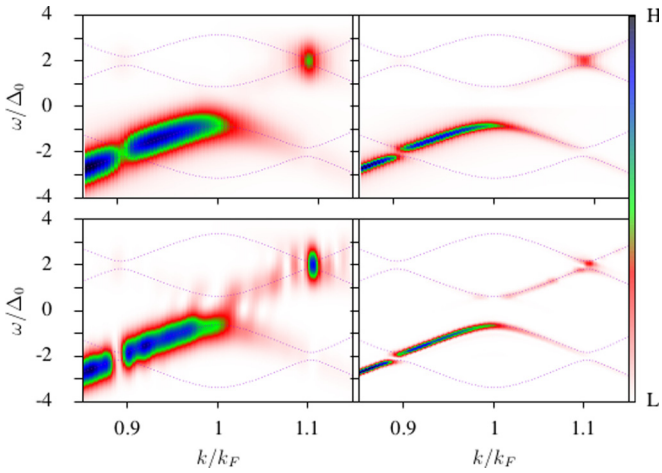

FIG. 7. tr-ARPES intensity for drive strength $\alpha = 0.2$, $t_0 = 0.75\tau_R$, and $\gamma = 0.2\Delta_0$ (upper panel) and $\gamma = 0$ (lower panel). We use a probe duration of $\sigma = 0.1\tau_R$ (left column) and $\sigma = 0.6\tau_R$ (right column). The dashed lines represent the quasienergy spectrum assuming a periodic time dependence $\Delta(t)$ as defined in the main text.

the superconducting gap shows several incommensurate frequencies (Rabi-Higgs and drive frequency) and Floquet theorem is not strictly applicable. For $\gamma = 0$, we compute the Floquet spectrum for a $\Delta(t) = 0.63\Delta_0 + 0.35\Delta_0 \cos(\omega_d t)$. Thus, the transient response shown in Fig. 6 and the lower panels in Fig. 7 can be seen as a time-dependent change in the occupancy of the Floquet band structure. Clearly, the reason this analysis works in the Rabi-Higgs oscillation regime is the large separation of time scales between the slow Rabi-Higgs dynamics and the fast drive oscillations [43].

B. Time-resolved tunneling experiment

We now discuss a possible setup to detect the Rabi-Higgs mode and the steady-state nonlinearities via tunneling measurements. In the last decades there have been efforts to add temporal resolution to scanning tunneling spectroscopy (STM) techniques and now subpicosenconds resolution can be reached in experimental setups [44–46]. In principle one can radiate a sample while performing the measurement making STM a feasible time resolved technique at the same level as pump-probe measurements [46]. However, since the spatial resolution is not a requirement to reveal these nonlinearities, a planar junction would probably be a more stable setting. An antenna could be used to couple the radiation with the superconductors as is done in detectors for photons with energy matching the superconducting gap [47,48]. In what follows, we will refer to STM signal but our formalism applies also for the case of a planar junction.

To obtain the STM signal, we now consider a tip located close above the out of equilibrium superconductor and tunnel coupled locally to the $\boldsymbol{k}$ states in the system. The entire problem can be described by a generic Hamiltonian $H = H_{\rm MF} + H_{\rm T} + H_{\rm TS}$ where we have added the tip (or metallic planar junction) Hamiltonian

$$H_{\rm T} = \sum_{\boldsymbol{p}} (\epsilon_{\boldsymbol{p}} + eV) a^\dagger_{\boldsymbol{p}} a_{\boldsymbol{p}}, \tag{23}$$

and the coupling between both subsystem via the tunneling Hamiltonian

$$H_{\rm TS} = \sum_{\boldsymbol{k},\boldsymbol{p}} (T_{\boldsymbol{kp}}\, c^\dagger_{\boldsymbol{k}} a_{\boldsymbol{p}} + \text{H.c.}). \tag{24}$$

The tip or the metallic contact is connected to an external voltage source with energy eV, $a_{\boldsymbol{p}}$ ($a^\dagger_{\boldsymbol{p}}$) destroys (creates) an electron with momentum $\boldsymbol{p}$ and energy $\epsilon_{\boldsymbol{p}} + eV$ in the tip and $T_{\boldsymbol{kp}}$ is the strength of the tunneling. The electron current operator is given by

$$\hat{I} = ie[\hat{N}, \hat{H}] = ie(\hat{L}^\dagger - \hat{L}), \tag{25}$$

where e is the electron charge, $\hat{N} = \sum_{\boldsymbol{p}} a^\dagger_{\boldsymbol{p}} a_{\boldsymbol{p}}$ is the number operator, and $\hat{L} = \sum_{\boldsymbol{k},\boldsymbol{p}} T_{\boldsymbol{kp}} c^\dagger_{\boldsymbol{k}} a_{\boldsymbol{p}}$. Assuming a response linear in $H_{\rm TS}$ (weak coupling between tip and superconductor) we calculate the current through the tip as

$$I(t) = ie \int_{-\infty}^{\infty} \theta(t - t') \langle [\hat{I}(t), H_{\rm TS}(t')] \rangle_0 \tag{26}$$

where $\langle ... \rangle_0$ denotes the expectation value at zero order in the tunneling Hamiltonian. Notice that we have not consider the spin degree of freedom so far as the current is a spin conserved quantity (not spin-flip are allowed in the tunneling process). This will be included in the final expression of the time-dependent current as a factor 2. From Eq. (26) we obtain

$$I(t) = 2eT^2 \int_{-\infty}^{t} dt' \sum_{\boldsymbol{k},\boldsymbol{p}} \Big(\big[e^{-i\epsilon_{\boldsymbol{p}}(t-t')} \langle c^\dagger_{\boldsymbol{k}}(t) c_{\boldsymbol{k}}(t') \rangle \Theta(\epsilon_{\boldsymbol{p}} - eV) - e^{i\epsilon_{\boldsymbol{p}}(t-t')} \langle c_{\boldsymbol{k}}(t) c^\dagger_{\boldsymbol{k}}(t') \rangle \Theta(-\epsilon_{\boldsymbol{p}} + eV) \big] + (t \leftrightarrow t') \Big), \tag{27}$$

where we have assumed a momentum-independent tunneling coupling $T_{\boldsymbol{kp}} \equiv T$ and a zero-temperature Fermi distribution for the electrons on the tip via the Heaviside step function $\Theta(x)$. Taking the derivative of Eq. (27) with respect to the voltage V and using Eq. (6), the time-dependent differential conductance can be written as

$$G(t) = \frac{dI}{dV} \propto \text{Im} \sum_{\boldsymbol{k}} \int_{-\infty}^{t} dt' \text{Tr}[\boldsymbol{G}^<_{\boldsymbol{k}}(t, t')] e^{-ieV(t-t')} \tag{28}$$

where Tr represents the trace in Nambu space. In the absence of the drive (that is, at equilibrium) the differential conductance becomes time independent, being proportional to the well-know phenomenological Dynes density of states

$$G \propto \rho(eV) = \rho_0 \,\text{Re}\left[\frac{eV + i\Gamma}{\sqrt{(eV + i\Gamma)^2 - \Delta_0^2}} \right], \tag{29}$$

where the Dynes parameter $\Gamma = \gamma/2$, Δ_0 is the equilibrium order parameter, and ρ_0 is the normal phase density of states. It is worth recalling that the Dynes formula was originally introduced phenomenologically [27]. There have been several theoretical proposals to provide a formal justification including Eliashberg physics [49], inelastic tunneling [50], and magnetic impurities [51,52]. In our previous work we have shown that the coupling with a bath [28] provides a mechanism to justify Dynes formula and allows us to link directly equilibrium tunneling with the γ parameter. Of course since we are not providing a microscopic theory of the bath our justification is still semiphenomenological.

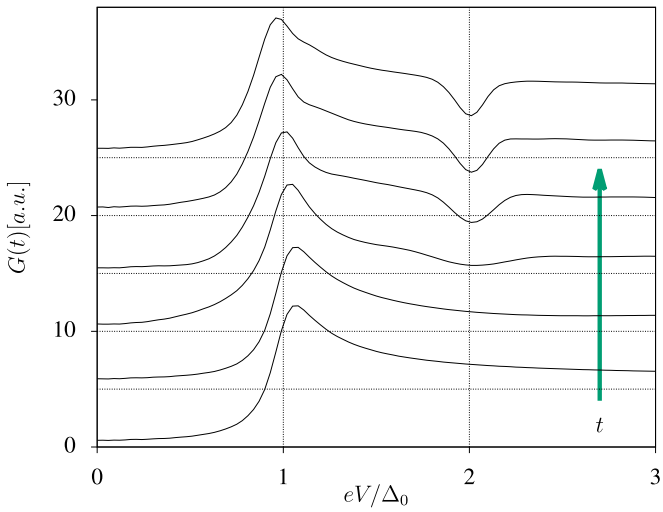

FIG. 8. Differential conductance for $\alpha = 0.1$ at several values of times inside the first period τ_R of Rabi-Higgs mode, from bottom to top, $t = 0$ (equilibrium), $t = 0.1\tau_R$, $t = 0.25\tau_R$, $t = 0.5\tau_R$, $t = 0.75\tau_R$, and $t = \tau_R$. We use $\gamma = 0.2\Delta_0$ and the zero for each curve (horizontal dashed line) was displaced by factor 5 for clarity.

Turning to the driven case, for small γ values the out-of-equilibrium differential conductance is computationally very demanding since the whole dynamics has to be integrated in Eq. (28), differently from the photoemission case where the integrals are cutoff by the probe pulse shape. To make the computations feasible we use $\gamma = 0.2\Delta_0$ and $\alpha = 0.1$. The nominal Rabi-Higgs period corresponds to $\tau_R\Delta_0 \approx 27$ but because of the large damping a steady state is reached before a full Rabi cycle is completed. Still as shown in Fig. 8, the time-dependent differential conductance clearly shows a nontrivial transient dynamics. Indeed, a clear depression in the time-resolved conductance around $eV = 2\Delta_0$ can be observed as a function of time which can be identified with the beginning of the Rabi-Higgs oscillation.

As in the case of photoemission two effects determine the features in the spectrum. The upper and lower Bogoliubov bands hybridize with the first Floquet sideband of the lower and upper Bogoliubov bands, respectively, creating a pseudogap at $\pm\omega_d/2$ (see right column of Fig. 7). Furthermore, the depression of the population at energy $-\omega_d/2$ depresses the probability to extract electrons and the excess of population at energy $\omega_d/2$ prevents injecting electrons due to Pauli blocking.

Another effect of the drive is that the whole shape of the conductance gets modified. Due to the Dynes parameter, at equilibrium the differential conductance does not vanishes sharply for energies lower than Δ_0. Once the time-dependent perturbation is turned on, the superconducting coherence peak decreases according to a decreasing in the average order parameter.

IV. SUMMARY AND OUTLOOK

We have studied the dynamic of a BCS superconductor subject to a periodic drive in the presence of dissipation focusing on possible nonlinear phenomena. An important effect of dissipation is that the Rabi-Higgs oscillations of Ref. [18] which persist forever when $\gamma = 0$, become a transient phenomenon and require $\gamma \lesssim \Omega_R$ to be observable. At long times $t \gtrsim 1/\gamma$, linear response is valid for a weak drive such that $\Omega_R \ll \Delta_0$, while steady-state nonlinearities such as the phenomenon of saturation of population imbalance, are obtained for large drives. Another interesting nonlinearity is second harmonic generation, which we have found is allowed for the peculiar symmetry of λ drive. We stress that except for this last result, all the other effects are expected to be universally present for other kinds of drives (DOS-driving, THz, and optical excitations, etc.).

Our system is very different form a single driven two-level system. Indeed, the Rabi oscillations are collective and involve a finite fraction of two-level systems thanks to interactions that produce synchronization. Notwithstanding that, there is a close analogy with the nonlinear regimes of a single two-level system which paves the way to explore quantum optics protocols taken to a collective level to control and manipulate the superconducting state of materials. We have identified two nonlinear regimes: a transient regime at short times in systems with long relaxation times and a steady-state regime. It is customary to consider "transient effects" as unimportant but one should keep in mind that practically all modern quantum technologies are based in such nonlinear transient phenomena and the problem of fighting decoherence effects, so its current importance cannot be overemphasized.

The experimental detection of these highly nonlinear behaviors in driven superconductors could be a major step towards the quantum control and manipulation of quantum phases. We have proposed tr-ARPES and time-resolved tunneling to detect Rabi-Higgs oscillations in the presence of dissipation. The time resolution required for these experiments is not necessary high and would depend on how long is the out-of-equilibrium relaxation time which limits the slower Rabi oscillations that can be seen. Assuming a Rabi-Higgs period on the order of $10^2/\Delta_0$, in superconducting aluminum thin films it corresponds to the range of 0.1 ns, which is much larger than usual tr-ARPES time resolution (typically ∼300 fs or in some cases ∼30 fs). It is also long with respect to the subpicosecond resolution achieved in some STM experiments [44–46].

In tr-ARPES, the excited quasiparticle population appears as a decrease (increase) in the photoemission intensity at energy $-\omega_d/2$ ($+\omega_d/2$) measured from the chemical potential. For the Rabi-Higgs mode this imbalance will change cyclically while for the steady-state nonlinear regime it should stabilize in a distribution compatible with the unbalance population seen in the momentum distribution function (Fig. 5) according to Eq. (20). In the last case, time resolution, of course would not be an issue. Remarkably, we have demonstrated that tr-ARPES signals match very well with a Floquet spectrum not only in the steady-state regime but also in the transient dynamics. The tunneling intensity should show an analogous cyclic time-dependent depression of intensity at $\pm\omega_d/2$ due to the lacking of spectral density and population unbalance causing Pauli blockade. This anomaly should stabilize at a reduced value at long times as a signature of the steady-state nonlinear behavior. We remark that also the detection of these

steady-state features would be of interest and does not require high temporal resolution.

We have previously proposed a phonon-assisted mechanism to induce periodic modulation of the pairing interaction in superconducting FeSe which represents a possible candidate to explore all nonlinear phenomena discussed here. The main idea is to excite a A_{1g} mode (oscillations of Se anions) which controls the pairing. Taking into account infrared light pulse with typical fluence values, the estimated α parameters in this case are <0.1 (see Ref. [18]). Here we used slightly larger values for technical reasons. On the other hand, the λ driving can also be implemented in ultracold atomic systems as discussed in the introduction. In this case, larger values of α could be explored.

The present formalism can be easily extended to take into account more interesting relaxation mechanisms via more sophisticated self-energies beyond the wide-band approximation used here for the bath. An interesting direction is to analyze how robust the Rabi-Higgs mode is in the presence of dephasing, decoherence, and relaxation sources from a more microscopic point of view by considering residual Coulomb and electron-phonon interactions where heating effects could be relevant.

ACKNOWLEDGMENTS

J.L. is in debt for enlightening discussions with L. Benfatto, C. Castellani, G. Seibold, B. Leridon, N. Bergeal, and Jérôme Lesueur. We acknowledge financial support from Italian MAECI and Argentinian MINCYT through bilateral project AR17MO7 and from ANPCyT (Grants No. PICTs 2013-1045 and No. 2016-0791), from CONICET (Grant No. PIP 11220150100506) and from SeCyT-UNCuyo (Grant No. 06/C603). J.L. acknowledges financial support from Italian MAECI thought collaborative project SUPERTOP-PGR04879, from Italian MIUR though Project No. PRIN 2017Z8TS5B, and from Regione Lazio (L. R. 13/08) under project SIMAP.

[1] D. Fausti, R. I. Tobey, N. Dean, S. Kaiser, A. Dienst, M. C. Hoffmann, S. Pyon, T. Takayama, H. Takagi, and A. Cavalleri, Light-induced superconductivity in a stripe-ordered cuprate, Science **331**, 189 (2011).

[2] B. Mansart, J. Lorenzana, A. Mann, A. Odeh, M. Scarongella, M. Chergui, and F. Carbone, Coupling of a high-energy excitation to superconducting quasiparticles in a cuprate from coherent charge fluctuation spectroscopy, Proc. Natl. Acad. Sci. **110**, 4539 (2013).

[3] R. Matsunaga, Y. I. Hamada, K. Makise, Y. Uzawa, H. Terai, Z. Wang, and R. Shimano, Higgs Amplitude Mode in the BCS Superconductors $Nb_{1-x}Ti_xN$ Induced by Terahertz Pulse Excitation, Phys. Rev. Lett. **111**, 057002 (2013).

[4] R. Matsunaga, N. Tsuji, H. Fujita, A. Sugioka, K. Makise, Y. Uzawa, H. Terai, Z. Wang, H. Aoki, and R. Shimano, Light-induced collective pseudospin precession resonating with Higgs mode in a superconductor, Science **345**, 1145 (2014).

[5] R. Mankowsky, A. Subedi, M. Först, S. O. Mariager, M. Chollet, H. T. Lemke, J. S. Robinson, J. M. Glownia, M. P. Minitti, A. Frano, M. Fechner, N. A. Spaldin, T. Loew, B. Keimer, A. Georges, and A. Cavalleri, Nonlinear lattice dynamics as a basis for enhanced superconductivity in $YBa_2Cu_3O_{6.5}$, Nature (London) **516**, 71 (2014).

[6] D. Nicoletti, E. Casandruc, Y. Laplace, V. Khanna, C. R. Hunt, S. Kaiser, S. S. Dhesi, G. D. Gu, J. P. Hill, and A. Cavalleri, Optically induced superconductivity in striped $La_{2-x}Ba_xCuO_4$ by polarization-selective excitation in the near infrared, Phys. Rev. B **90**, 100503(R) (2014).

[7] S. Kaiser, C. R. Hunt, D. Nicoletti, W. Hu, I. Gierz, H. Y. Liu, M. Le Tacon, T. Loew, D. Haug, B. Keimer, and A. Cavalleri, Optically induced coherent transport far above Tc in underdoped $YBa_2Cu_3O_{6+x}$, Phys. Rev. B **89**, 184516 (2014).

[8] M. Mitrano, A. Cantaluppi, D. Nicoletti, S. Kaiser, A. Perucchi, S. Lupi, P. Di Pietro, D. Pontiroli, M. Riccò, S. R. Clark, D. Jaksch, and A. Cavalleri, Possible light-induced superconductivity in K_3C_{60} at high temperature, Nature (London) **530**, 461 (2016).

[9] S. Rajasekaran, J. Okamoto, L. Mathey, M. Fechner, V. Thampy, G. D. Gu, and A. Cavalleri, Probing optically silent superfluid stripes in cuprates, Science **359**, 575 (2018).

[10] T. Stöferle, H. Moritz, C. Schori, M. Köhl, and T. Esslinger, Transition from a Strongly Interacting 1D Superfluid to a Mott Insulator, Phys. Rev. Lett. **92**, 130403 (2004).

[11] E. Haller, R. Hart, M. J. Mark, J. G. Danzl, L. Reichsöllner, M. Gustavsson, M. Dalmonte, G. Pupillo, and H. C. Nägerl, Pinning quantum phase transition for a Luttinger liquid of strongly interacting bosons, Nature (London) **466**, 597 (2010).

[12] M. Endres, T. Fukuhara, D. Pekker, M. Cheneau, P. Schauß, C. Gross, E. Demler, S. Kuhr, and I. Bloch, The 'Higgs' amplitude mode at the two-dimensional superfluid/Mott insulator transition, Nature (London) **487**, 454 (2012).

[13] C. Chin, R. Grimm, P. Julienne, and E. Tiesinga, Feshbach resonances in ultracold gases, Rev. Mod. Phys. **82**, 1225 (2010).

[14] A. Behrle, T. Harrison, J. Kombe, K. Gao, M. Link, J.-S. Bernier, C. Kollath, and M. Köhl, Higgs mode in a strongly interacting fermionic superfluid, Nat. Phys. **14**, 781 (2018).

[15] L. W. Clark, L.-C. Ha, C.-Y. Xu, and C. Chin, Quantum Dynamics with Spatiotemporal Control of Interactions in a Stable Bose-Einstein Condensate, Phys. Rev. Lett. **115**, 155301 (2015).

[16] R. A. Barankov and L. S. Levitov, Synchronization in the BCS Pairing Dynamics as a Critical Phenomenon, Phys. Rev. Lett. **96**, 230403 (2006).

[17] M. Eckstein, M. Kollar, and P. Werner, Thermalization after an Interaction Quench in the Hubbard Model, Phys. Rev. Lett. **103**, 056403 (2009).

[18] H. P. O. Collado, J. Lorenzana, G. Usaj, and C. A. Balseiro, Population inversion and dynamical phase transitions in a driven superconductor, Phys. Rev. B **98**, 214519 (2018).

[19] A. F. Volkov and Sh. M. Kogan, Collisionless relaxation of the energy gap in superconductors, Zh. Eksp. Teor. Fiz. **65**, 2038 (1973) [Sov. Phys. JETP **38**, 1018 (1974)].

[20] R. A. Barankov, L. S. Levitov, and B. Z. Spivak, Collective Rabi Oscillations and Solitons in a Time-Dependent BCS Pairing Problem, Phys. Rev. Lett. **93**, 160401 (2004).

[21] J. Lorenzana, B. Mansart, A. Mann, A. Odeh, M. Chergui, and F. Carbone, Investigating pairing interactions with coherent charge fluctuation spectroscopy, Eur. Phys. J. Spec. Top. **222**, 1223 (2013)..

[22] C. A. Balseiro and L. M. Falicov, Phonon Raman Scattering in Superconductors, Phys. Rev. Lett. **45**, 662 (1980).

[23] P. B. Littlewood and C. M. Varma, Amplitude collective modes in superconductors and their coupling to charge-density waves, Phys. Rev. B **26**, 4883 (1982).

[24] T. Cea, C. Castellani, and L. Benfatto, Nonlinear optical effects and third-harmonic generation in superconductors: Cooper pairs versus higgs mode contribution, Phys. Rev. B **93**, 180507(R) (2016).

[25] D. A. Steck, *Quantum and Atom Optics*, available online at http://steck.us/teaching (2019).

[26] E. G. Mishchenko, Dynamic Conductivity in Graphene Beyond Linear Response, Phys. Rev. Lett. **103**, 246802 (2009).

[27] R. C. Dynes, V. Narayanamurti, and J. P. Garno, Direct Measurement of Quasiparticle-Lifetime Broadening in a Strong-Coupled Superconductor, Phys. Rev. Lett. **41**, 1509 (1978).

[28] H. P. Ojeda Collado, G. Usaj, J. Lorenzana, and C. A. Balseiro, Fate of dynamical phases of a bcs superconductor beyond the dissipationless regime, Phys. Rev. B **99**, 174509 (2019).

[29] O. P. Saira, A. Kemppinen, V. F. Maisi, and J. P. Pekola, Vanishing quasiparticle density in a hybrid Al/Cu/Al single-electron transistor, Phys. Rev. B **85**, 012504 (2012).

[30] J. J. Chang and D. J. Scalapino, Nonequilibrium superconductivity, J. Low Temp. Phys. **31**, 1 (1978).

[31] M. A. Sentef, A. F. Kemper, A. Georges, and C. Kollath, Theory of light-enhanced phonon-mediated superconductivity, Phys. Rev. B **93**, 144506 (2016).

[32] A.-P. Jauho, N. S. Wingreen, and Y. Meir, Time-dependent transport in interacting and noninteracting resonant-tunneling systems, Phys. Rev. B **50**, 5528 (1994).

[33] H. M. Pastawski, Classical and quantum transport from generalized landauer-büttiker equations. ii. time-dependent resonant tunneling, Phys. Rev. B **46**, 4053 (1992).

[34] T. Xu, T. Morimoto, A. Lanzara, and J. E. Moore, Efficient prediction of time- and angle-resolved photoemission spectroscopy measurements on a nonequilibrium bcs superconductor, Phys. Rev. B **99**, 035117 (2019).

[35] D. M. Kennes, E. Y. Wilner, D. R. Reichman, and A. J. Millis, Nonequilibrium optical conductivity: General theory and application to transient phases, Phys. Rev. B **96**, 054506 (2017).

[36] T. Cea, P. Barone, C. Castellani, and L. Benfatto, Polarization dependence of the third-harmonic generation in multiband superconductors, Phys. Rev. B **97**, 094516 (2018).

[37] A. Ferrón, D. Domínguez, and M. J. Sánchez, Tailoring Population Inversion in Landau-Zener-Stückelberg Interferometry of Flux Qubits, Phys. Rev. Lett. **109**, 237005 (2012).

[38] J. K. Freericks, H. R. Krishnamurthy, and T. Pruschke, Theoretical Description of Time-Resolved Photoemission Spectroscopy: Application to Pump-Probe Experiments, Phys. Rev. Lett. **102**, 136401 (2009).

[39] J. H. Shirley, Solution of the schrödinger equation with a hamiltonian periodic in time, Phys. Rev. **138**, B979 (1965).

[40] H. Sambe, Steady states and quasienergies of a quantum-mechanical system in an oscillating field, Phys. Rev. A **7**, 2203 (1973).

[41] S. Kohler, J. Lehmann, and P. Hänggi, Driven quantum transport on the nanoscale, Phys. Rep. **406**, 379 (2005).

[42] M. Grifoni and P. Hanggi, Driven quantum tunneling, Phys. Rep. **304**, 229 (1998).

[43] L. Peralta Gavensky, G. Usaj, and C. A. Balseiro, Time-resolved hall conductivity of pulse-driven topological quantum systems, Phys. Rev. B **98**, 165414 (2018).

[44] M. Morgenstern, STM ready for the time domain, Science **329**, 1609 (2010).

[45] G. Nunes and M. R. Freeman, Picosecond resolution in scanning tunneling microscopy, Science **262**, 1029 (1993).

[46] O. Takeuchi, M. Aoyama, R. Oshima, Y. Okada, H. Oigawa, N. Sano, H. Shigekawa, R. Morita, and M. Yamashita, Probing subpicosecond dynamics using pulsed laser combined scanning tunneling microscopy, Appl. Phys. Lett. **85**, 3268 (2004).

[47] J. Zmuidzinas and H. G. LeDuc, Quasi-optical slot antenna sis mixers, IEEE Transactions on Microwave Theory and Techniques **40**, 1797 (1992).

[48] B. Leridon, Josephson noise in quasiparticle mixers, J. Appl. Phys. **81**, 3243 (1997).

[49] A. Mikhailovsky, S. Shulga, A. Karakozov, O. Dolgov, and E. Maksimov, Thermal pair-breaking in superconductors with strong electron-phonon interaction, Solid State Communications **80**, 511 (1991).

[50] J. P. Pekola, V. F. Maisi, S. Kafanov, N. Chekurov, A. Kemppinen, Y. A. Pashkin, O.-P. Saira, M. Möttönen, and J. S. Tsai, Environment-Assisted Tunneling as an Origin of the Dynes Density of States, Phys. Rev. Lett. **105**, 026803 (2010).

[51] F. Herman and R. Hlubina, Microscopic interpretation of the dynes formula for the tunneling density of states, Phys. Rev. B **94**, 144508 (2016).

[52] F. Herman and R. Hlubina, Thermodynamic properties of dynes superconductors, Phys. Rev. B **97**, 014517 (2018).